

Vibration overtone hyperpolarizability measured for H₂

Cite as: J. Chem. Phys. 152, 154301 (2020); doi: 10.1063/5.0005233

Submitted: 18 February 2020 • Accepted: 25 March 2020 •

Published Online: 16 April 2020



View Online



Export Citation



CrossMark

Rachel M. Ellis  and David P. Shelton ^{a)} 

AFFILIATIONS

Department of Physics and Astronomy, University of Nevada, Las Vegas, Nevada 89154-4002, USA

^{a)} Author to whom correspondence should be addressed: shelton@physics.unlv.edu

ABSTRACT

The second hyperpolarizability (γ) of the H₂ molecule was measured by gas-phase electric field induced second harmonic generation at the frequencies of the one-photon resonance for the 3–0 Q(J) overtone transitions ($v, J = 0, J \rightarrow 3, J$ for $J = 0, 1, 2$, and 3). The magnitude of the resonant contribution to γ was measured with 2% accuracy using the previously determined non-resonant γ for calibration. Pressure broadening and frequency shift for the transitions were also measured. A theoretical expression for the resonant vibrational γ contribution in terms of transition polarizabilities is compared to the observations. The measured γ resonance strength is 4%–14% larger than the results obtained from this theoretical expression evaluated using *ab initio* transition polarizabilities.

Published under license by AIP Publishing. <https://doi.org/10.1063/5.0005233>

I. INTRODUCTION

The nonlinear optical (NLO) response of a centrosymmetric molecule is described by the second hyperpolarizability tensor $\gamma_{\alpha\beta\gamma\delta}(-\omega_{\sigma}; \omega_1, \omega_2, \omega_3)$, which is a complicated function of the incident field frequencies $\omega_1, \omega_2, \omega_3$ and polarizations β, γ, δ due to the electronic, vibrational, and rotational excitations of the molecule.¹ The electronic hyperpolarizability contribution can be simply described by a universal dispersion formula that applies for all NLO processes,^{1,2} but the expressions for the vibrational hyperpolarizability are more complicated and differ significantly from one NLO process to the next.^{3,4}

For the special case of a homonuclear diatomic molecule, a simple expression for the vibrational hyperpolarizability has been derived, which gives the vibrational hyperpolarizability in terms of the vibrational transition polarizabilities for the molecule, and applies for all NLO processes.⁵ For a homonuclear diatomic molecule, using this expression to calculate the vibrational hyperpolarizability, the electronic hyperpolarizability can be determined from hyperpolarizability dispersion measurements for one NLO process. This then allows the dispersion curve for any other NLO processes to be determined. Such an analysis has been applied to hyperpolarizability measurements for H₂, D₂, N₂, and O₂.⁶ However, some approximations are made in the derivation of

this expression for the vibrational hyperpolarizability, and a direct experimental test of the expression has not been performed since the vibrational and electronic contributions are not distinguished in the usual experiments measuring the total molecular hyperpolarizability. Since the electronic and vibrational contributions are defined by their resonance frequencies, the resonant response of the vibrational hyperpolarizability can be used to unequivocally distinguish it from the electronic hyperpolarizability. The $\Delta v = 3$ overtone transitions in H₂ fall in the frequency range accessible with an available Ti:sapphire laser, and for H₂ there is no dipole-allowed absorption to impede a measurement of the resonant vibrational hyperpolarizability. In the following, the theoretical expression for the resonant vibrational hyperpolarizability is presented, the experiment to measure the resonant overtone vibrational hyperpolarizability in H₂ is described, and the experimental results are used to test the theoretical expression for the vibrational hyperpolarizability.

II. THEORY

The second hyperpolarizability of a non-polar molecule is given by the following sum-over-states expression:^{5,7–9}

$$\gamma_{\alpha\beta\gamma\delta}(-\omega_\sigma; \omega_1, \omega_2, \omega_3) = \hbar^{-3} \sum_P \left\{ \begin{array}{l} \sum_{m,n,p(\neq g)} \frac{\langle g|\mu_\alpha|m\rangle\langle m|\mu_\delta|n\rangle\langle n|\mu_\gamma|p\rangle\langle p|\mu_\beta|g\rangle}{(\omega_{mg} - \omega_\sigma)(\omega_{ng} - \omega_1 - \omega_2)(\omega_{pg} - \omega_1)} \\ - \sum_{m,p(\neq g)} \frac{\langle g|\mu_\alpha|m\rangle\langle m|\mu_\delta|g\rangle\langle g|\mu_\gamma|p\rangle\langle p|\mu_\beta|g\rangle}{(\omega_{mg} - \omega_\sigma)(\omega_{pg} - \omega_1)(\omega_{pg} + \omega_2)} \end{array} \right\}, \quad (1)$$

where $\omega_\sigma = \omega_1 + \omega_2 + \omega_3$, $|g\rangle$ is the initial (ground) state of the molecule, μ_α is the α Cartesian component of the electric dipole operator, and \sum_P denotes the summation of the 24 terms obtained by permuting the frequencies $-\omega_\sigma, \omega_1, \omega_2, \omega_3$ along with the associated spatial indices $\alpha, \beta, \gamma, \delta$ that specify the molecular frame Cartesian components of the induced dipole and the applied electric fields. The terms in this expression can be partitioned into rotational, vibrational, or electronic contributions according to whether the lowest resonance frequency for the term is a rotational, vibrational, or electronic transition frequency. For homonuclear diatomic molecules such as H_2 , the dipole matrix elements between rovibronic states in the ground electronic manifold vanish by symmetry, so the only non-vanishing contributions to the vibrational hyperpolarizability γ^v are terms in the first group in Eq. (1), where the intermediate state $|n\rangle$ is a rovibrational state in the ground electronic manifold. The resulting expression for the vibrational hyperpolarizability of a homonuclear diatomic molecule is⁵

$$\gamma_{\alpha\beta\gamma\delta}^v(-\omega_\sigma; \omega_1, \omega_2, \omega_3) = \hbar^{-3} \sum_P \sum_{n(\neq g)} \frac{1}{(\omega_{ng} - \omega_1 - \omega_2)} \times \left\{ \sum_{m(\neq g)} \frac{\langle g|\mu_\alpha|m\rangle\langle m|\mu_\delta|n\rangle}{(\omega_{mg} - \omega_\sigma)} \right\} \times \left\{ \sum_{p(\neq g)} \frac{\langle n|\mu_\gamma|p\rangle\langle p|\mu_\beta|g\rangle}{(\omega_{pg} - \omega_1)} \right\}, \quad (2)$$

where ω_{ng} is a rovibrational transition frequency, ω_{mg} and ω_{pg} are electronic transition frequencies, and the factors in braces have the form of transition polarizabilities.

An expression for the vibrational hyperpolarizability of a gas of homonuclear diatomic molecules for any third order nonlinear optical process [Eq. (17) in Ref. 5] is obtained from Eq. (2) by making the approximation that optical frequencies are negligible compared to electronic transition frequencies in the transition polarizability factors, summing over permutations, and evaluating the isotropic average. The isotropic averaged hyperpolarizability tensor for electric field induced second harmonic generation (ESHG) has two independent components $\gamma_{||} = \langle \gamma(-2\omega; \omega, \omega, 0) \rangle_{XXXX}$ and $\gamma_{\perp} = \langle \gamma(-2\omega; \omega, \omega, 0) \rangle_{YYXX}$, with optical and static electric fields polarized either parallel or perpendicular, respectively. From Eq. (17) in Ref. 5, the one-photon resonance contribution to the ESHG vibrational hyperpolarizability due to a Q branch vibration transition, near resonance where $|\omega_{0J,vJ} - \omega| \ll \omega$, is given by

$$\gamma_{||,Q}^v = \rho(J) \frac{2}{\hbar(\omega_{0J,vJ} - \omega)} \left[\alpha_{0J,vJ}^2 + \frac{4}{45} \frac{J(J+1)}{(2J-1)(2J+3)} \Delta\alpha_{0J,vJ}^2 \right], \quad (3)$$

$$\gamma_{\perp,Q}^v = \rho(J) \frac{2}{\hbar(\omega_{0J,vJ} - \omega)} \left[\frac{1}{15} \frac{J(J+1)}{(2J-1)(2J+3)} \Delta\alpha_{0J,vJ}^2 \right], \quad (4)$$

where $\alpha = (\alpha_{||} + 2\alpha_{\perp})/3$ and $\Delta\alpha = (\alpha_{||} - \alpha_{\perp})$ are the mean and anisotropy of the transition polarizabilities for light polarized $||$ or \perp to the molecular axis for the selected Q branch transition with resonance frequency, $\omega_{0J,vJ}$, and $\rho(J)$ is the fractional population of rotational level J . Similar expressions are obtained for the O and S branch transitions with frequencies $\omega_{0J,vJ\pm 2}$,

$$\gamma_{||,O}^v = (4/3)\gamma_{||,O}^v = \rho(J) \frac{2}{\hbar(\omega_{0J,vJ-2} - \omega)} \left[\frac{2}{15} \frac{J(J-1)}{(2J-1)(2J+1)} \Delta\alpha_{0J,vJ-2}^2 \right], \quad (5)$$

$$\gamma_{||,S}^v = (4/3)\gamma_{||,S}^v = \rho(J) \frac{2}{\hbar(\omega_{0J,vJ+2} - \omega)} \left[\frac{2}{15} \frac{(J+1)(J+2)}{(2J+1)(2J+3)} \Delta\alpha_{0J,vJ+2}^2 \right]. \quad (6)$$

Equations (3)–(6) are obtained by neglecting optical frequencies in the polarizability factors in braces in Eq. (2). A better estimate of frequency dispersion, without this approximation, can be made if one considers only the terms in Eq. (2) near one-photon resonance for a single vibration transition frequency ω_{ng} . Selecting just those terms, ignoring spatial indices $\alpha\beta\gamma\delta$, writing out the 24 frequency permutations for ESHG, relabeling dummy indices, and collecting terms gives the following expression:

$$\gamma_{res}^v(-2\omega; \omega, \omega, 0) = \frac{2}{\hbar(\omega_{ng} - \omega)} \left\{ \sum_{m(\neq g)} \frac{2\mu_{gm}\mu_{mn}}{\hbar(\omega_{mg} + 2\omega)} \right\} \times \left\{ \sum_{p(\neq g)} \frac{2\mu_{gp}\mu_{pn}}{\hbar(\omega_{pg} - \omega)} \right\}. \quad (7)$$

The tensor $\gamma_{\alpha\beta\gamma\delta}^v$ for H_2 ESHG has seven independent components ($\alpha\beta\gamma\delta = zzzz, zxzx, xzxx, zzxx, xxzz, xyxx, \text{ and } xxxx$, where z is the molecular axis). Equation (7) is the exact result for the $zzzz$ and $xxxx$ components of $\gamma_{\alpha\beta\gamma\delta}^v$, where all permutations of $\alpha\beta\gamma\delta$ are the same. The other components have more complicated expressions with the same resonance denominators. The polarizability factors in braces in Eq. (7) can be compared to the expressions for the static polarizability α_0 ,

$$\alpha_0 = \sum_{m(\neq g)} \left\{ \frac{2\mu_{gm}\mu_{mn}}{\hbar\omega_{mg}} \right\}, \quad (8)$$

and the Raman polarizability α_R ,¹⁰

$$\alpha_R(-\omega_S; \omega_P) = \sum_{m(\neq g)} \left\{ \frac{\mu_{gm}\mu_{mn}}{\hbar(\omega_{mg} + \omega_S)} + \frac{\mu_{gm}\mu_{mn}}{\hbar(\omega_{mg} - \omega_P)} \right\}, \quad (9)$$

where ω_P is the pump frequency and $\omega_S = \omega_P - \omega_{ng}$ is the Stokes frequency for Raman scattering. The effective polarizability α_γ for γ_{res}^v is the square root of the product of the two transition polarizabilities appearing in Eq. (7). The dispersion for α_γ is given by the geometric mean of factors with resonance denominators $(\omega_{mg} + 2\omega)$ and $(\omega_{mg} - \omega)$, whereas the dispersion of α_R is given by the arithmetic mean of terms with resonance denominators $(\omega_{mg} + \omega_S)$ and $(\omega_{mg} - \omega_P)$. The resonance denominators in Eqs. (7) and (9) indicate that the Raman polarizability α_R will increase with increasing frequency ω_P since $\omega_S < \omega_P$, whereas α_γ will decrease with increasing ω (when $\omega_{mg} > 4\omega$) since $2\omega > \omega$.

To deal with zero detuning from resonance, the usual phenomenological imaginary damping $i\Gamma$ term is added to the resonance denominators in Eqs. (3)–(6), giving complex hyperpolarizabilities $\gamma^v = \gamma_R^v + i\gamma_I^v$. Equation (3) for Q branch transitions becomes

$$\gamma_{\parallel,Q}^v = 2\hbar^{-1}\rho(J)\left[\alpha_{0J,vJ}^2 + \frac{4}{45}\frac{J(J+1)}{(2J-1)(2J+3)}\Delta\alpha_{0J,vJ}^2\right] \times \left[\frac{(\omega_{0J,vJ} - \omega) - i\Gamma}{(\omega_{0J,vJ} - \omega)^2 + \Gamma^2}\right]. \quad (10)$$

The observed second harmonic signal near a vibrational resonance is $S^{(2\omega)} \propto |\gamma|^2$ where the total hyperpolarizability γ is the sum of the complex resonant vibrational hyperpolarizability and the slowly varying non-resonant real hyperpolarizability due to all other contributions,

$$S^{(2\omega)} \propto |\gamma_{nr} + \gamma_{res}^v|^2 = (\gamma_{nr} + \gamma_{res,R}^v)^2 + (\gamma_{res,I}^v)^2. \quad (11)$$

The signal variation near resonance is determined by the relative size of the resonant and non-resonant contributions,

$$S^{(2\omega)}/S_{nr}^{(2\omega)} = (1 + \gamma_{res,R}^v/\gamma_{nr})^2 + (\gamma_{res,I}^v/\gamma_{nr})^2, \quad (12)$$

so the resonant hyperpolarizability γ_{res}^v can be calibrated in terms of γ_{nr} .

III. EXPERIMENT

The electric field induced second harmonic generation (ESHG) apparatus used in the present gas phase H_2 vibration overtone hyperpolarizability measurements is similar to that previously described.^{6,11–13} A coherent beam of second harmonic light is generated by the laser beam in a H_2 gas sample when a transverse static electric field is applied to the gas. The static electric field distorts the molecule and breaks centrosymmetry, allowing optical second harmonic generation even from spherically symmetric systems such as an atom or H_2 in the $J = 0$ rotational state. The spatially alternating static electric field applied to the gas is produced by a periodic array of N electrode pairs, and the ESHG signal is enhanced by a factor N^2 when the coherence length in the gas is adjusted to match the longitudinal period of the electrode array. To make an overtone signal measurement, the gas density ρ is first adjusted to set the coherence

length equal to the array period when the laser frequency is at the vibration overtone frequency. Then, with the gas density held constant at this value, the second harmonic signal is measured as the laser frequency is scanned over a 2 cm^{-1} range around the vibration overtone frequency. Four Q-branch $\Delta v = 3$ transitions near $\lambda = 850\text{ nm}$ were measured.

Figure 1 shows a schematic diagram of the apparatus. The cw ring Ti:sapphire laser (Ti:S) produces a frequency tunable single longitudinal mode (SLM) output beam with power about 400 mW in the 850 nm wavelength range. The laser beam is collimated by lens L1, the desired linear polarization state is prepared by the half wave plate (HWP) and prism polarizer (POL), lens L2 focuses the beam to a waist in the center of the gas cell with 20 cm confocal parameter, and the red glass filter (RG645) blocks any light at the second harmonic wavelength that may be present in the incident beam before it enters the gas cell (CELL). ESHG occurs as the laser beam passes between the electrodes in the gas cell (Fig. 1, inset). The transmitted fundamental beam and coaxial second harmonic beam generated in the gas cell are collimated by lens L3 and then separated by using the tandem Brewster prism spectrometer (P1, P2). The narrow second harmonic beam is expanded by lens L4 before reaching the photocathode of the photon counting photomultiplier tube (PMT). The quantum efficiency of the bi-alkali photocathode at the 850 nm laser wavelength is so low that sufficient rejection of the fundamental laser beam is achieved using just the double prism spectrometer without any additional spectral filters.

The laser frequency, power, and mode were continuously monitored during the ESHG measurements. About 1% of the laser beam is reflected by each of three beam samplers (BS1, BS2, and BS3). The beam sample from BS1 is divided by using beam splitter BS4 and then fiber-coupled to a Burleigh WA-20 wavemeter (WM) to measure the laser frequency and to a scanning Fabry Perot interferometer (FP) to monitor the laser mode. The beam sample from BS2 is focused by using lens L5 onto a 5 GHz InGaAs photodiode (PD) feeding a RF spectrum analyzer monitoring the beat note spectrum of the laser output. Since second harmonic generation (SHG) measurements are sensitive to mode composition,^{14,15} measurements were rejected if the appearance of an inter-mode beat note indicated that the laser was not producing SLM output. The final beam sample from BS3 goes to an integrating sphere (IS) and photodetector, to produce an output which is proportional to the laser power

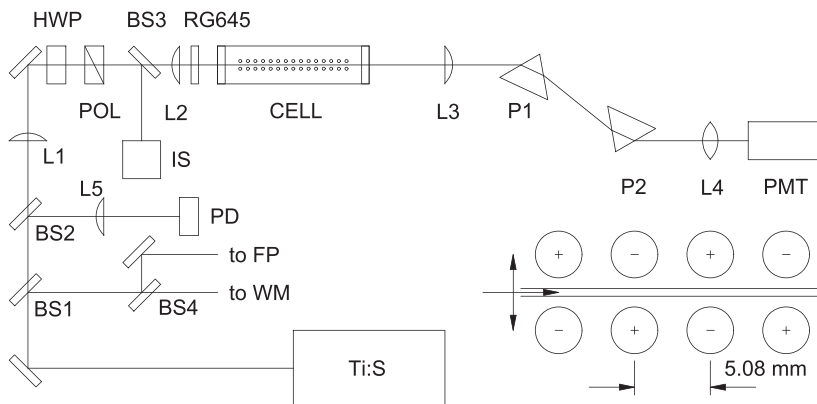


FIG. 1. Schematic diagram of the apparatus described in the text. The inset shows the path of the focused linear polarized laser beam between the alternating polarity cylindrical electrodes in the gas cell.

P actually reaching the gas cell during the ESHG measurement. For each ESHG measurement, P was determined from the average of multiple power measurements and $S^{(2\nu)}/P^2$ was computed to account for the effect of beam power fluctuations. BS3 is placed after HWP and POL so that etalon effects in these components, which can cause uncontrolled changes in beam transmission, do not corrupt the power measurement. To prevent etalon effects in the beam path after BS3, all of the following components are tilted or wedged so that no reflected beams overlap and L4 is inserted to diverge and expand the signal beam onto the photocathode, disrupting possible etalon fringes at the PMT entrance window.

Second harmonic generation by the laser beam at the surfaces of prism P1 is not forbidden by symmetry, and such a coherent SHG background could cause ESHG measurement errors. The observed signal in the presence of coherent background is $S_{\pm} \propto (\pm E_s + E_b \cos \phi)^2$, where $\pm E_s$ and $E_b \cos \phi$ are the electric field amplitudes of the ESHG signal and the coherent SHG background, respectively, and \pm indicates the two choices for the polarity of the voltage applied to the electrode array. The electric field between every pair of electrodes changes sign when the array polarity is reversed. This changes the sign but not the magnitude of the ESHG signal E_s . The relative amplitude of the coherent background was determined from the ratio of signals S_+/S_- , measured with forward and reversed array voltage, using the expression $E_b \cos \phi/E_s = (1/4)(S_+/S_- - 1)$. The measured amplitude for the coherent background is negligible, $|E_b \cos \phi/E_s| < 0.07\%$.

Figure 2 shows a scan of the ESHG signal spectrum for the H_2 Q(1) overtone transition, with the sharp vibration resonance riding on the much broader phase match peak. The functional form of the broad peak can be calculated by numerical integration of the phase match integral given in Refs. 6 and 12 using the electrode array and laser beam parameters for this experiment. The electrode array has $N = 82$ pairs of electrodes with period 5.08 mm, similar to array 1 in Ref. 13, and the confocal parameter of the focused laser beam

is 20 cm. The normalized phase match peak obtained by numerical integration is approximated by the function

$$g(\nu) = 1 - x^2 + 0.42x^4 - 0.10x^6, \quad (13)$$

where $x = (\nu - \nu_m)/w$ and $w \approx 54 \text{ cm}^{-1}$. The peak position ν_m and width w are parameters determined by fitting Eq. (13) to the phase match peak measurements, and the broad curve in Fig. 2 is the function $S_m g(\nu)$ fit to the off-resonance data. The gas density at phase match varies as $\rho_m \propto \nu_m^{-3}$,¹² and for each experiment, the gas density is adjusted to place ν_m within about 1 cm^{-1} of the molecular resonance frequency. The phase match function $g(\nu)$ multiplies the resonance signal function, and when ν_m is placed within 1 cm^{-1} of the resonance frequency, the variation of $g(\nu)$ over the resonance measurement range is $< 0.2\%$. Phase match at $\lambda = 850 \text{ nm}$ is obtained with H_2 gas density $\rho = 406 \text{ mol m}^{-3}$ (9.11 amagat). The typical off-resonance photon count signal was 300 s^{-1} for laser power 400 mW and static electric field 6 kV/mm, and the 0.6 s^{-1} PMT background count rate measured with zero static field was subtracted from this signal.

The resonance signal shown in Fig. 2 is measured at closely spaced points over an interval of about 2 cm^{-1} around resonance. The fit to the resonance data uses the following function based on Eq. (12):

$$f(\nu) = \left[1 + \frac{a(b - \nu)}{(b - \nu)^2 + c^2} \right]^2 + \left[\frac{ac}{(b - \nu)^2 + c^2} \right]^2, \quad (14)$$

where a is the relative magnitude of the resonant and nonresonant hyperpolarizabilities, b is the resonance frequency, c is the resonance width, and a , b , and c are parameters to be determined from the experimental observations. The experimental units are cm^{-1} for ν , a , b , and c . The observed second harmonic signal is given by the product of Eqs. (13) and (14),

$$S^{(2\nu)}/P^2 = Af(\nu)g(\nu). \quad (15)$$

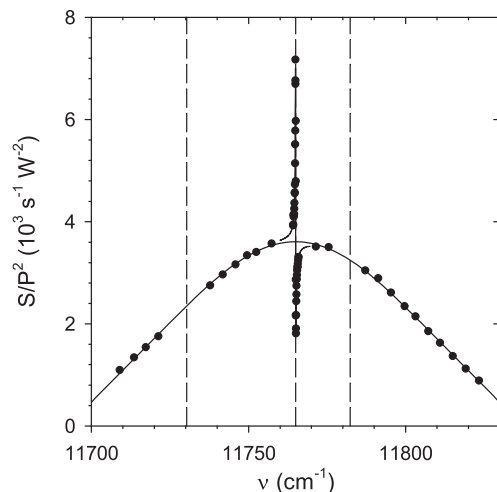


FIG. 2. ESHG signal vs frequency measured for the H_2 3–0 Q(1) transition. The solid curves are fits of Eqs. (13) and (15) to the data points. The vertical dashed lines mark the frequencies of the Q(2), Q(1), and Q(0) resonances.

IV. RESULTS AND DISCUSSION

The results of measurements for the 3–0 Q(J) overtone transitions for $J = 0, 1, 2$, and 3 are shown in Fig. 3. Each graph shows the combined results of multiple complete scans for each resonance. Separate scans of a resonance were combined by first fitting Eq. (15) to the $S^{(2\nu)}/P^2$ data for each scan and then computing and combining the normalized and baseline corrected data $f(\nu) = [S^{(2\nu)}/P^2]/[Ag(\nu)]$ for each scan. Figures 3(a)–3(e) show the combined data for 3, 3, 1, 3, and 2 separate scans, respectively. The frequency sequence in each scan was shuffled to reduce the effect of slow signal drift during the course of the measurements, and 2, 2, 0, 2, 1 of the scans in Figs. 3(a)–3(e) were also done by “triplets.” For these scans, a point about 0.4 – 1.0 cm^{-1} off-resonance was designated as the internal reference for the scan and measurements at other frequencies designated as the signal. Reference and signal measurements were alternated, and each signal measurement was normalized using the average of the reference measurements immediately before and after that signal measurement.

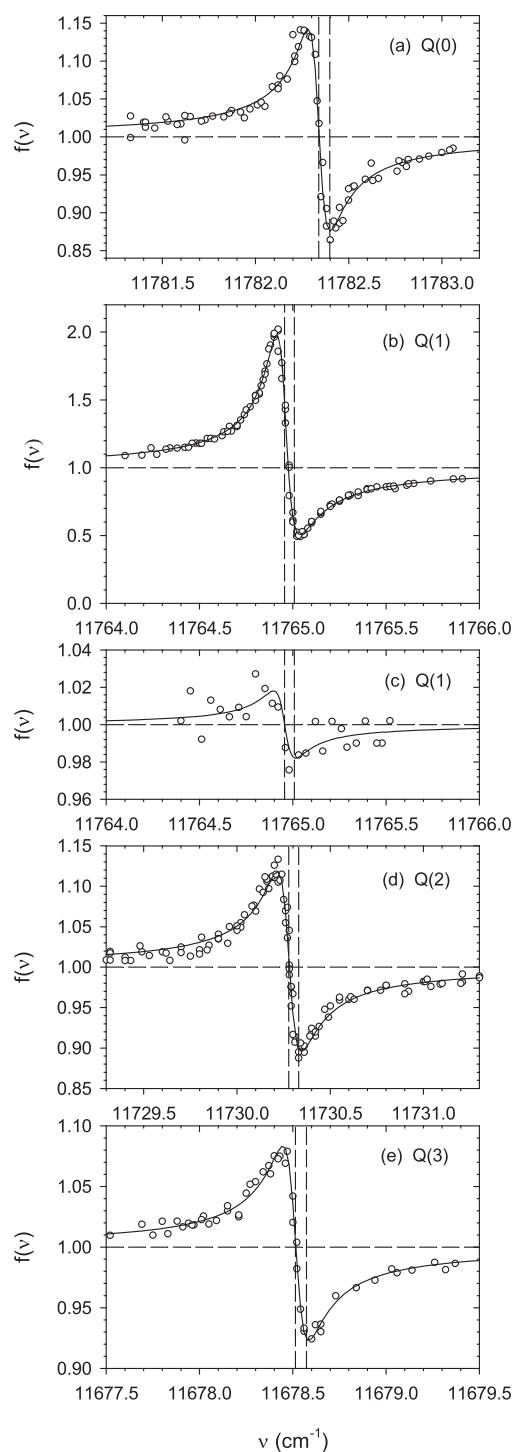


FIG. 3. Overtone resonance spectra over 2 cm^{-1} for H_2 transitions (a) Q(0), [(b) and (c)] Q(1), (d) Q(2), and (e) Q(3), measured with parallel polarization, except for (c) measured with \perp polarization. The solid curves are fits of Eq. (14) to the data points. The vertical dashed lines mark the measured and the *ab initio* resonance frequencies, and the horizontal dashed lines mark the non-resonant background level.

Table I gives the fit parameters obtained by fitting Eq. (14) to the combined data for each resonance. As outlined above, special care was taken to eliminate or account for any trend in the baseline underlying each resonance to prevent a systematic error in the resonance strength parameter a . The $0.001\text{--}0.003 \text{ cm}^{-1}$ precision obtained for the resonance position and width parameters b and c determined by the fits to the data is 3–10 times better than the 0.01 cm^{-1} absolute frequency accuracy of the wavemeter. Photon counting statistics accounts for about half of the total variance of the data points around the fit curves, except for the Q(1) resonance with laser beam polarization perpendicular to the static field in the cell, as shown in Fig. 3(c), where the signal is 10 times smaller and the variance is dominated by photon counting statistics. For the fit to this spectrum, the position and width for the resonance were set to the values determined for the same resonance with parallel polarization and only the resonance strength parameter a was determined from the fit to the data. The O and S branch transitions were not measured since the signal for these transitions was expected to be too weak, comparable to, or smaller than the signal for the corresponding Q branch transitions with perpendicular polarization.

Hydrogen gas at the pressure used in the present measurements is well into the collision broadening regime, where the resonance frequency shift and width are proportional to pressure.¹⁶ Table II gives the pressure shift and broadening coefficients calculated from the present measurements and a comparison with other previous measurements for H_2 gas.^{17,18} The frequency shift is determined from the resonance frequency b measured in the present experiment using the *ab initio* result for the vibration transition frequency of an isolated H_2 molecule as the frequency in the limit of zero pressure broadening.¹⁹ The *ab initio* result in Table II for the 1–0 Q(0) transition ($v, J = 0, 0 \rightarrow 1, 0$) differs from the experiment by 0.002 cm^{-1} , and by just 0.0002 cm^{-1} when relativistic and QED effects are included.²⁰ A similar comparison of experiment and theory for the 3–0 S(3) transition gives a difference of 0.0003 cm^{-1} ,²¹ with collisional line shape effects accounting for 0.0001 cm^{-1} of the difference.²² The pressure shift coefficients given in Table II for the 3–0 Q(J) transitions are determined assuming that the *ab initio* frequencies for these transitions are also accurate at the 0.002 cm^{-1} level, while the accuracy for the experimental frequencies from the present work is 0.01 cm^{-1} . Figure 4 shows the trend of the frequency shift and broadening coefficients as functions of the transition frequency. The pressure shift $(3.8 \pm 0.1) \times 10^{-3} \text{ cm}^{-1}/\text{atm}$ recently measured for

TABLE I. Parameters from the fit of Eq. (14) to the H_2 overtone resonance spectra in Fig. 3.

| Transition | a (10^{-3} cm^{-1}) | b (cm^{-1}) | c (10^{-3} cm^{-1}) |
|------------|-----------------------------------|--------------------------|-----------------------------------|
| 3–0 Q(0) | 7.85 ± 0.27 | $11\,782.338 \pm 0.001$ | 58.9 ± 2.5 |
| 3–0 Q(1) | 40.87 ± 0.65 | $11\,764.956 \pm 0.001$ | 59.1 ± 1.0 |
| 3–0 Q(1) | 1.06 ± 0.17^a | | |
| 3–0 Q(2) | 7.20 ± 0.26 | $11\,730.278 \pm 0.001$ | 64.9 ± 2.5 |
| 3–0 Q(3) | 5.49 ± 0.23 | $11\,678.513 \pm 0.002$ | 68.5 ± 2.9 |

^a \perp polarization.

TABLE II. Pressure shift and broadening coefficients measured for H₂ vibration transitions.

| Transition | ν_0^a (cm ⁻¹) | ρ^b (amagat) | $(\nu_0 - b)/\rho^c$ (10 ⁻³ cm ⁻¹ amagat ⁻¹) | c/ρ^d (10 ⁻³ cm ⁻¹ amagat ⁻¹) |
|------------|----------------------------------|----------------------|---|---|
| 1-0 Q(0) | 4 161.168 4 | | | 1.33 ± 0.01 |
| 1-0 Q(1) | 4 155.254 7 | | 2.13 ± 0.04 | 0.87 ± 0.04 |
| 1-0 Q(2) | 4 143.466 0 | | 2.0 ± 0.1 | 1.48 ± 0.01 |
| 1-0 Q(3) | 4 125.873 9 | | 2.2 ± 0.2 | 1.21 ± 0.01 |
| 1-0 Q(4) | 4 102.582 0 | | 1.7 ± 1.9 | 1.71 ± 0.03 |
| 1-0 Q(5) | 4 073.732 7 | | | 1.17 ± 0.03 |
| 2-0 Q(1) | 8 075.311 4 | | 4.8 ± 0.2 | |
| 2-0 Q(2) | 8 051.991 0 | | 4 ± 3 | |
| 2-0 Q(3) | 8 017.190 0 | | 4 ± 4 | |
| 3-0 Q(0) | 11 782.397 1 | 9.059 | 6.6 ± 1.1 | 6.5 ± 0.3 |
| 3-0 Q(1) | 11 765.007 8 | 9.108 | 5.7 ± 1.1 | 6.5 ± 0.1 |
| 3-0 Q(2) | 11 730.331 8 | 9.192 | 5.9 ± 1.1 | 7.1 ± 0.3 |
| 3-0 Q(3) | 11 678.572 1 | 9.328 | 6.3 ± 1.1 | 7.3 ± 0.3 |

^a ν_0 from Ref. 19.

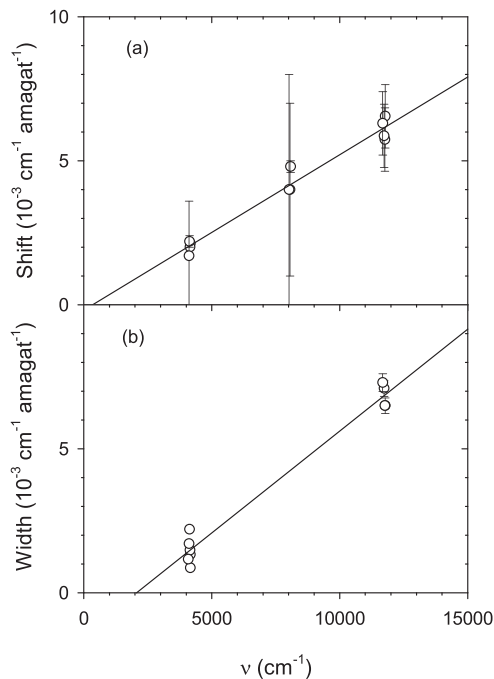
^b1 amagat = $\rho_{STP} = 44.588$ mol/m³ for H₂ gas.

^cShift for 1-0 and 2-0 from Ref. 17.

^dBroadening for 1-0 from Ref. 18.

the 3-0 S(3) transition is about half as large as the shift for the 3-0 Q(3) transition.²¹

The calculated relative strength a of the vibrational hyperpolarizability resonances measured in this experiment is determined


FIG. 4. Pressure shift (a) and broadening (b) coefficients plotted vs Q branch transition frequency. Lines fit to the data are a guide to the eye.

by the effective transition polarizability α_{eff} and the non-resonant hyperpolarizability γ_{nr} at the transition frequency. From Eqs. (3), (4), (10), (12), and (14), one has

$$a_{calc} = 2\rho(J)\alpha_{eff}^2 e_H / \gamma_{nr}, \quad (16)$$

where $\rho(J) \propto (2J + 1)g_{ns}(J)\exp(-E_{0J}/k_B T)$ is the fractional population of rotational level J of the ground state at temperature T and $e_H = 219\,474.6307$ cm⁻¹/hartree converts energy difference $\hbar(\omega_{0J,vJ} - \omega)$ from atomic units to cm⁻¹. For Q branch transitions with parallel optical and static field polarization,

$$\alpha_{eff,\parallel}^2 = \left[\alpha_{0J,vJ}^2 + \frac{4}{45} \frac{J(J+1)}{(2J-1)(2J+3)} \Delta\alpha_{0J,vJ}^2 \right], \quad (17)$$

and for Q branch transitions with perpendicular field polarization,

$$\alpha_{eff,\perp}^2 = \left[\frac{1}{15} \frac{J(J+1)}{(2J-1)(2J+3)} \Delta\alpha_{0J,vJ}^2 \right]. \quad (18)$$

The rotational level populations $\rho(J)$ were calculated using the energy levels from the *ab initio* calculation in Ref. 19, and α_{eff}^2 was calculated using the *ab initio* static transition polarizabilities from Ref. 23. A subsequent *ab initio* calculation of α_{eff}^2 for the Raman 3-0 Q(1) transition¹⁰ is in good agreement with the earlier static result.²³ The non-resonant hyperpolarizability γ_{nr} is obtained using the expression fit to previous 0.5% accurate ESHG measurements made for H₂ over a wide frequency range with parallel polarization,⁶

$$\gamma_{nr} = \gamma_0(1 + B\nu_L^2 + C\nu_L^4) + G\nu^{-2} + H\nu^{-4}, \quad (19)$$

where $\nu_L^2 = 6\nu^2$ for ESHG, $\gamma_0 = 686.41$ a.u., $B = 1.200 \times 10^{-10}$ cm², $C = 2.254 \times 10^{-20}$ cm⁴, $G = -2.552 \times 10^9$ a.u. cm⁻², and $H = -3.997 \times 10^{16}$ a.u. cm⁻⁴. The G and H terms are an approximation for the

off-resonance rovibrational hyperpolarizability that differs from the explicit sum over rovibrational transitions by <0.1 a.u. in the frequency region of the present work. For the Q(1) transition measured with perpendicular polarization, the reference γ_{nr} is obtained using Eq. (19) and the value $\gamma_{\parallel}/\gamma_{\perp} = 2.909$ from the H₂ ESHG measurements in Ref. 24. Table III gives the results a_{calc} of this calculation and a comparison with the measured results a_{expt} . The experimental results are all larger than the calculated results, and the average of the results weighted by the experimental uncertainties is 1.040 ± 0.013 for the ratios a_{expt}/a_{calc} .

Static transition polarizabilities were used to calculate the results in Table III, and a possible reason for the discrepancy between the calculated and experimental results is the neglect of the frequency dependence of the polarizabilities in the theoretical calculation. To estimate the frequency dispersion, one can approximate each sum over excited electronic states appearing in Eqs. (7)–(9) by a single term with an effective electronic excitation energy. The effective electronic excitation energy can be obtained by fitting approximate Eq. (9) to the polarizability dispersion calculated in Ref. 10 for the 1–0 Q(1) H₂ Raman transition. The *ab initio* Raman polarizability at $\hbar\omega = 0.10$ a.u. is 1.094 times larger than the static polarizability, and the fit to this dispersion value gives an effective electronic transition frequency $\nu_{eg} = 82\,000$ cm⁻¹ (0.374 a.u.). Using the single term approximation with $\nu_{eg} = 82\,000$ cm⁻¹ for the polarizabilities in Eq. (7), one estimates that α_{ν} at 11 765 cm⁻¹ is reduced to 0.95 times its static value so that the values for a_{calc} in Table III are overestimates by 10%, and the discrepancy between theory and experiment is actually 14% rather than 4%. This result from the present experiment indicates that the *ab initio* polarizabilities for the $\Delta\nu = 3$ transitions are 2%–7% too small. Also consistent with the present result, the previously measured value for the 3–0 Q(1) Raman transition polarizability²⁵ is 5% larger than the *ab initio* value.¹⁰ Negative dispersion that is deduced for the polarizability α_{ν} is unexpected, but the *ab initio* calculation for the $\Delta\nu = 3$ overtone Raman polarizability also exhibits small negative dispersion due to the combined effects of mechanical anharmonicity and strong frequency dependence of the polarizability second derivative.¹⁰ Further support for the conclusion that the 3–0 Q(J) polarizabilities are larger than the *ab initio* calculated values comes

from a Morse potential model calculation for H₂ that gives values for the high overtone polarizabilities that are orders of magnitude higher than the extrapolated results of *ab initio* calculations²⁶ and also from recent experiments selectively populating high vibrational states of H₂ that are fit by a polarizability more than an order of magnitude larger than the *ab initio* polarizability for the $\Delta\nu = 4$ transition.²⁷

The hyperpolarizability contribution from the 3–0 Q(1) transition reaches maximum magnitude $|\gamma^v| = 515$ a.u. on resonance but decreases to ± 0.26 a.u. just 100 cm⁻¹ off-resonance. In comparison, the rovibrational contribution to the nonresonant hyperpolarizability is $\gamma_{nr}^{vr} = -20.5$ a.u. at the 3–0 Q(1) resonance frequency and is dominated by the far off-resonance contribution of the fundamental vibration transition. There is good agreement between calculations for the fundamental transition polarizabilities,^{10,28} but the frequency dependence of the effective polarizabilities appearing in the expression for γ_{nr}^{vr} is uncertain. The expression for γ_{nr}^{vr} is based on Eq. (17) of Ref. 5, which was obtained by neglecting the frequency dependence of the polarizability factors in Eq. (2). A simple expression such as Eq. (7) is not obtained for γ^v far off-resonance. The dispersion of the effective polarizability in γ_{nr}^{vr} may be significant, as suggested by the Raman polarizability at $\nu_P = 11\,765$ cm⁻¹ for the 1–0 Q(1) transition, which is 1.044 times the static polarizability.¹⁰ This dispersion would produce a 10% increase in the calculated value for γ_{nr}^{vr} at this frequency. An indication that the dispersion for the effective polarizability may be less than that for α_R comes from the comparison of accurate experimental ESHG and *ab initio* results for γ of H₂ at $\nu = 19\,430$ cm⁻¹,¹³ where the experiment and theory agree with $\pm 0.1\%$ uncertainty. This sets a bound on the possible error for the calculated vibrational hyperpolarizability γ_{nr}^{vr} , which contributes 0.74% of γ at this frequency. Agreement within 0.1% indicates that the increase in γ_{nr}^{vr} due to the effective polarizability dispersion is $<14\%$ at this frequency. The uncertainty for γ_{nr}^{vr} does not affect the accuracy of the vibrational resonance hyperpolarizability calibration in terms of γ_{nr} in the present work. The uncertainty for γ_{nr}^{vr} affects the partition of γ_{nr} into electronic and rovibrational contributions but not the total, since Eq. (19) for γ_{nr} is the sum of the two contributions adjusted to fit the experimental γ_{nr} data.

TABLE III. Comparison of calculated and experimental overtone vibration resonance relative strength a at $T = 296$ K. Atomic units are used for α , $\Delta\alpha$ (1 a.u. = $1.648\,778 \times 10^{-41}$ C² m² J⁻¹), and γ_{nr} (1 a.u. = $6.235\,377 \times 10^{-65}$ C⁴ m⁴ J⁻³).

| J | $\rho(J)^a$ | α^b (10 ⁻² a.u.) | $\Delta\alpha^b$ (10 ⁻² a.u.) | γ_{nr}^c (a.u.) | a_{calc} (10 ⁻³ cm ⁻¹) | a_{expt}/a_{calc} |
|-----|-------------|------------------------------------|--|------------------------|---|--------------------------|
| 0 | 0.1304 | 0.993 | -0.567 | 745.3 | 7.57 | 1.037 ± 0.034 |
| 1 | 0.6596 | 0.997 | -0.568 | 745.0 | 39.08 | 1.046 ± 0.016 |
| 1 | 0.6596 | 0.997 | -0.568 | 256.1 ^{d,e} | 0.97 ^d | 1.11 ± 0.16 ^d |
| 2 | 0.1164 | 1.004 | -0.568 | 744.3 | 6.98 | 1.032 ± 0.036 |
| 3 | 0.0887 | 1.014 | -0.567 | 743.3 | 5.43 | 1.011 ± 0.042 |

^aUsing rotational energy levels from Ref. 19.

^bStatic transition polarizabilities from Ref. 23.

^cUsing Eq. (19).

^d_⊥ polarization.

^eUsing $\gamma_{\parallel}/\gamma_{\perp} = 2.909$ at this frequency from Ref. 24.

V. CONCLUSION

This experiment measured the second overtone vibrational contribution to the second hyperpolarizability of H₂ and found that the measured strength of the observed resonance is 4%–14% larger than predicted using the transition polarizabilities from high level *ab initio* calculations. This experiment determines the transition polarizability with accurate absolute calibration provided by the nonresonant hyperpolarizability previously determined for the molecule. This method could be used to measure overtone transition polarizabilities for other small molecules.

DATA AVAILABILITY

The data that support the findings of this study are available from the corresponding author upon reasonable request.

REFERENCES

- ¹D. P. Shelton and J. E. Rice, *Chem. Rev.* **94**, 3 (1994).
- ²D. M. Bishop and D. W. De Kee, *J. Chem. Phys.* **104**, 9876 (1996).
- ³D. M. Bishop, *Adv. Chem. Phys.* **104**, 1 (1998).
- ⁴D. M. Bishop, J. M. Luis, and B. Kirtman, *J. Chem. Phys.* **108**, 10013 (1998).
- ⁵D. P. Shelton, *Mol. Phys.* **60**, 65 (1987).
- ⁶D. P. Shelton, *Phys. Rev. A* **42**, 2578 (1990).
- ⁷B. J. Orr and J. F. Ward, *Mol. Phys.* **20**, 513 (1971).
- ⁸Y. R. Shen, *The Principles of Nonlinear Optics* (Wiley, New York, 1984).
- ⁹P. N. Butcher and D. Cotter, *The Elements of Nonlinear Optics* (Cambridge University Press, Cambridge, 1990).
- ¹⁰D. M. Bishop and J. Pipin, *J. Chem. Phys.* **94**, 6073 (1991).
- ¹¹V. Mizrahi and D. P. Shelton, *Phys. Rev. A* **32**, 3454 (1985).
- ¹²D. P. Shelton and V. Mizrahi, *Phys. Rev. A* **33**, 72 (1986).
- ¹³E. A. Donley and D. P. Shelton, *Chem. Phys. Lett.* **215**, 156 (1993); **228**, 701 (1994).
- ¹⁴S. Helmfrid and G. Arvidsson, *J. Opt. Soc. Am. B* **8**, 2326 (1991).
- ¹⁵W.-L. Zhou, Y. Mori, T. Sasaki, and S. Nakai, *Jpn. J. Appl. Phys.* **34**, 5606 (1995).
- ¹⁶A. Owyong, *Opt. Lett.* **2**, 91 (1978).
- ¹⁷S. L. Bragg, W. H. Smith, and J. W. Brault, *Astrophys. J.* **263**, 999 (1982).
- ¹⁸L. A. Rahn, R. L. Farrow, and G. J. Rosasco, *Phys. Rev. A* **43**, 6075 (1991).
- ¹⁹K. Pachucki and J. Komasa, *J. Chem. Phys.* **130**, 164113 (2009).
- ²⁰G. D. Dickenson, M. L. Niu, E. J. Salumbides, J. Komasa, K. S. E. Eikema, K. Pachucki, and W. Ubachs, *Phys. Rev. Lett.* **110**, 193601 (2013).
- ²¹C.-F. Cheng, Y. R. Sun, H. Pan, J. Wang, A.-W. Liu, A. Campargue, and S.-M. Hu, *Phys. Rev. A* **85**, 024501 (2012).
- ²²P. Wcislo, I. E. Gordon, C.-F. Cheng, S.-M. Hu, and R. Ciurylo, *Phys. Rev. A* **93**, 022501 (2016).
- ²³J. L. Hunt, J. D. Poll, and L. Wolniewicz, *Can. J. Phys.* **62**, 1719 (1984).
- ²⁴D. P. Shelton and Z. Lu, *Phys. Rev. A* **37**, 2231 (1988).
- ²⁵D. P. Shelton, *J. Chem. Phys.* **93**, 1491–1495 (1990).
- ²⁶S. Chelkowski and A. D. Bandrauk, *J. Raman Spectrosc.* **28**, 459 (1997).
- ²⁷W. E. Perreault, N. Mukherjee, and R. N. Zare, *J. Chem. Phys.* **145**, 154203 (2016).
- ²⁸A. Raj, H.-O. Hamaguchi, and H. A. Witek, *J. Chem. Phys.* **148**, 104308 (2018).